



LAWRENCE
LIVERMORE
NATIONAL
LABORATORY

Magnetic Field Advection in Two Interpenetrating Plasma Streams

D. D. Ryutov, N. L. Kugland, M. Levy, C. Plechaty,
J. S. Ross, H. S. Park

December 13, 2012

The Physics of Plasmas

Disclaimer

This document was prepared as an account of work sponsored by an agency of the United States government. Neither the United States government nor Lawrence Livermore National Security, LLC, nor any of their employees makes any warranty, expressed or implied, or assumes any legal liability or responsibility for the accuracy, completeness, or usefulness of any information, apparatus, product, or process disclosed, or represents that its use would not infringe privately owned rights. Reference herein to any specific commercial product, process, or service by trade name, trademark, manufacturer, or otherwise does not necessarily constitute or imply its endorsement, recommendation, or favoring by the United States government or Lawrence Livermore National Security, LLC. The views and opinions of authors expressed herein do not necessarily state or reflect those of the United States government or Lawrence Livermore National Security, LLC, and shall not be used for advertising or product endorsement purposes.

**MAGNETIC FIELD ADVECTION IN TWO INTERPENETRATING
PLASMA STREAMS**

D. D. Ryutov, N. L. Kugland, M.C. Levy, C. Plechaty, J. S. Ross, and H. S. Park

Lawrence Livermore National Laboratory, Livermore, CA 94551, USA

Abstract

Laser-generated colliding plasma streams can serve as a test-bed for the study of various astrophysical phenomena and the general physics of self-organization. For streams of a sufficiently high kinetic energy, collisions between the ions of one stream with the ions of the other stream are negligible, and the streams can penetrate through each other. On the other hand, the intra-stream collisions for high-Mach-number flows can still be very frequent, so that each stream can be described hydrodynamically. Presented in this paper is an analytical study of the effects that these interpenetrating streams have on large-scale magnetic fields either introduced by external coils or generated in the plasma near the laser targets. Specifically, a problem of the frozen-in constraint (“Into which stream is the magnetic field frozen?”) is resolved and paradoxical features of the field advection in this system are revealed. A possibility of using this system for studies of magnetic reconnection is mentioned.

I. INTRODUCTION

Two laser-generated interpenetrating plasma streams can serve as a test-bed for the study of various astrophysical phenomena [1] and of the general physics of self-organization [2]. For streams of a sufficiently high kinetic energy, collisions of the ions of one stream with the ions of the other stream are negligible, and the streams can penetrate through one another [1, 3]. If the spatial scale of the area where the streams overlap is sufficiently large, one may observe the formation of collisionless shocks mediated by the development of plasma microturbulence [4-7]. For experiments with a smaller-sized overlap zone, the microturbulence does not have a chance to develop, and the ion streams penetrate through each other more-or-less freely [3]. Our paper is pertinent to this latter regime of freely interpenetrating ion streams.

The collisions within each stream can be still very frequent. Indeed, the streams in the experiments of the type described in [2, 3] are produced by the free expansion of a plasma created by the interaction of a laser light with a target. The initial thermal energy is converted to the kinetic energy of the expanding flow. The electrons and ions cool down in this process, and a very high-Mach-number flow is formed [8]. Since the temperature of each stream is low, collisions between the ions within each stream and between electrons and ions are very frequent, so that the electron gas and the ions within each stream are highly collisional. Various effects of these intra-stream collisions have been studied in Refs. [9, 10].

Note that in the present paper we have switched from the term “jet” used in some previous publications on interpenetrating plasmas [8, 9], to the term “streams,” as the flows used in the aforementioned experiments are less collimated than the jets produced in dedicated experiments on astrophysically-relevant jets (e.g., [11, 12]). Therefore, the term “stream” seems to better relate the properties of the plasma flows with which we are concerned.

We will address the issue of magnetic field line-tying and magnetic field advection in a system comprised of two such interpenetrating plasma streams. We consider large-scale fields either imposed by external sources, or generated in the streams themselves (e.g., by the “ $\nabla n_e \times \nabla T_e$ ” mechanism acting in the hot-plasma zone near the targets [13]). As the magnetic Reynolds number is typically high (see below), one might expect that the frozen-in condition for the magnetic field would hold, and the magnetic flux would be advected in the plasma flow. However, the presence of the interpenetrating streams makes the situation somewhat more complex than usual, as one can ask: “Into which stream is the magnetic field frozen?” In this study, we assess this problem in a two-fluid dynamics framework, using the quasineutrality constraint and the electron momentum equation. We find the streamlines of the effective flow, into which the field is frozen, and provide some examples of the magnetic field advection. We allow for the streams to be made of different elements, with charge states Z_1 and Z_2 and the corresponding atomic masses A_1 and A_2 .

In our numerical estimates, we use the set of parameters for each stream as given in Table 1, assuming that the streams are identical and have a common axis (Fig 1). However, the general equations presented in this paper are free of these assumptions.

II. THE ELECTRON MOMENTUM EQUATION

As is well known (e.g., Ref. [13]), to assess the magnetic advection, one has to analyze the electron momentum equation. We note that the electron collision mean-free path is much shorter than the characteristic spatial scale, so that one can use the Braginski momentum equation. Moreover, the electron thermal velocity is much higher than directed ion velocity and ion thermal velocity. The characteristic time τ (Table 1) is much longer than the electron transit time L/v_{Te} (Table 2), thus allowing us to neglect the electron inertia term. With these observation made, one can write down the following electron momentum equation (see Eq. (2.2e) in Ref. [14]):

$$0 = -\nabla(n_e T_e) - en_e \left(\mathbf{E} + \frac{\mathbf{v}_e \times \mathbf{B}}{c} \right) + \mathbf{F}_T + \mathbf{F}_{ei}. \quad (1)$$

As mentioned, we neglect the inertial terms in the left-hand side; we also neglect the electron viscosity, as it is very small compared to, say, the electron-ion friction terms. The retained terms in Eq. (1) have the following meaning: the first term is the pressure gradient, the second is the Lorentz force, the third is the electron thermal force, and the last term describes the electron friction against the ions (Cf. Refs. 13,14).

The friction force is proportional to the plasma resistivity; the latter does not affect the magnetic field evolution, since the magnetic Reynolds number (Table 2) is very large. So, we can neglect the last term in Eq. (1).

The thermal force can be represented as ([14], Eq. (4.31)):

$$\mathbf{F}_T = n_e \left(-\alpha_{\parallel} \nabla_{\parallel} T_e - \alpha_{\perp} \nabla_{\perp} T_e - \alpha_{\wedge} \mathbf{b} \times \nabla T_e \right), \quad (2)$$

where $\mathbf{b} \equiv \mathbf{B}/B$ is a unit vector in the magnetic field direction, and the coefficients α depend significantly on the electron magnetization, by which we mean the ratio of the electron mean-free path to the electron gyro-radius, λ_{ei}/ρ_e . The last term in Eq. (2) describes the component of the force perpendicular to both the magnetic field and the electron temperature gradient (“Nernst effect”). For the plasma parameters presented in Tables 1 and 2, the magnetization parameter is less than one only for very low magnetic fields, below 2 to 3 kG.

For weak magnetic fields, where the magnetization parameter is small (“weak magnetization”) an expression for the thermal force, up to the first-order terms in the magnetization parameter, reads as:

$$\mathbf{F}_T \approx -0.71 n_e \nabla T_e - \alpha_1 n_e \frac{e \mathbf{B} \times \nabla T_e}{mc v_{ei}}, \quad (3)$$

where α_1 is a numerical parameter of order 1. The first term here appeared from the first two terms in Eq. (2), due to the fact that the coefficients α_{\parallel} and α_{\perp} become equal to each other for $\lambda_{ei}/\rho_e \rightarrow 0$. As has been correctly pointed out in Ref. [15], the Nernst effect may impact the advection of magnetic fields in laser-generated plasmas under some circumstances.

For a high magnetization, $\lambda_{ei}/\rho_e \gg 1$, the expression for the thermal force, up to the terms of the first order in the parameter $\rho_e/\lambda_{ei} \ll 1$ becomes [14]:

$$\mathbf{F}_T \approx -0.71 n_e \nabla_{\parallel} T_e - \alpha_2 n_e \left(\frac{\rho_e}{\lambda_{ei}} \right) \mathbf{b} \times \nabla T_e, \quad (4)$$

where α_2 is another coefficient of order one. For strong magnetization, the Nernst term is negligible (see numerical estimates below).

After this preparatory work, we can proceed to the solution of the advection problem. To do so, we find \mathbf{E} from Eq. (1) and substitute it in the Faraday equation, $\partial \mathbf{B} / \partial t = -c \nabla \times \mathbf{E}$. In this way we obtain that

$$\partial \mathbf{B} / \partial t = \nabla \times [\mathbf{v}_e \times \mathbf{B}] + \frac{c}{en_e} [\nabla n_e \times \nabla T_e] + \frac{c}{e} \nabla \times \frac{\mathbf{F}_T}{n_e}. \quad (5)$$

As mentioned above, we have neglected the electron-ion friction. If retained, it would have led to a magnetic diffusion term in the r.h.s. that is negligibly small for the set of parameters of Table 1.

Now we relate the electron velocity and the ion velocity. We use the quasineutrality constraint,

$$n_e = \sum_k Z_i^{(k)} n_i^{(k)}, \quad (6)$$

where the superscript “ k ” refers to the k -th stream, and we allow for having streams made of different ion species. We also use a straightforward expression for the current density:

$$\mathbf{j} = -en_e \mathbf{v}_e + e \sum_k Z_i^{(k)} n_i^{(k)} \mathbf{v}_i^{(k)}. \quad (7)$$

From the last two equations we have:

$$\mathbf{v}_e = -\frac{\mathbf{j}}{en_e} + \mathbf{u}, \quad (8)$$

with

$$\mathbf{u} = \frac{\sum_k Z_i^{(k)} n_i^{(k)} \mathbf{v}_i^{(k)}}{\sum_k Z_i^{(k)} n_i^{(k)}} \quad (9)$$

Note that the velocity \mathbf{u} coincides with the ion mass velocity of the ion flow only in the case where the ratio Z_i/A_i is the same for all jets. One can call velocity \mathbf{u} “the ion charge velocity.” By an order of magnitude, it is equal to the velocity \mathbf{v} that enters Table 1.

The electron continuity equation has a standard form $\partial n_e / \partial t + \nabla \cdot (n_e \mathbf{v}_e) = 0$ or, due to the quasineutrality condition,

$$\frac{\partial n_e}{\partial t} + \nabla \cdot (n_e \mathbf{u}) = 0 \quad (10)$$

The first term in the right-hand side (rhs) of Eq. (8) is responsible for the Hall effect. Let us estimate the relative magnitude of the first and the second terms in Eq. (8). As $\mathbf{j} = (c/4\pi) \nabla \times \mathbf{B}$, we can estimate j as $j \sim cB/4\pi L$, so that the ratio of the first term to the second term becomes “1”/“2” $\sim cB/4\pi en_e vL$. Substituting numerical values from Table 1, we find: “1”/“2” $\sim B/100\text{MG}$. A field of 100 MG cannot be generated by the system under consideration, in particular, because of a simple energy consideration (the field energy density would greatly exceed the plasma energy density). So, we conclude that one can neglect the first term compared to the second term in Eq. (8). One can note in passing that, if the Hall term was dominant, one would have entered the regime of so-called Hall magnetohydrodynamics, or electron magnetohydrodynamics [16], with very different advection properties.

The last term in Eq. (5) can be presented as:

$$\frac{c}{e} \nabla \times \frac{\mathbf{F}_T}{n_e} = -\frac{c}{e} \nabla \times (\alpha_{\parallel} \nabla_{\parallel} T_e + \alpha_{\perp} \nabla_{\perp} T_e) + \nabla \times [\mathbf{u}_N \times \mathbf{B}], \quad (11)$$

where

$$\mathbf{u}_N = \frac{c\alpha_{\perp}}{eB} \nabla T_e \quad (12)$$

is a quantity of the dimension of velocity arising from the Nernst term in the thermal force.

Neglecting the term proportional to j in Eq. (8) and using Eqs (11), (12), one arrives at the following equation describing the evolution of the magnetic field:

$$\partial \mathbf{B} / \partial t = \nabla \times [(\mathbf{u} + \mathbf{u}_N) \times \mathbf{B}] + \mathbf{S}, \quad (13)$$

where

$$\mathbf{S} = \frac{c}{e} \left\{ \frac{[\nabla n_e \times \nabla T_e]}{n_e} + \nabla \times (\alpha_{\parallel} \nabla_{\parallel} T_e + \alpha_{\perp} \nabla_{\perp} T_e) \right\}. \quad (14)$$

Equation (13) describes advection of the magnetic field in a medium that moves with the velocity $\mathbf{u} + \mathbf{u}_N$; the term \mathbf{S} is a source term. In a weakly magnetized plasma, one has [14]: $\alpha_{\parallel} = \alpha_{\perp} = 0.71$, and the vorticity term in Eq. (14) drops out. We recover then the standard $\nabla n_e \times \nabla T_e$ source. [Note that the numerical values of the α 's depend on the ion charge; the coefficient 0.71 refers to hydrogen; for carbon it is close to 1.2, see Table 2 in Ref. [14]. In a highly magnetized plasma, α_{\perp} becomes negligibly small, leading to an order one modification of the source term.

The main focus of this paper is to consider new features of the advection effect in the presence of two (or more) interpenetrating ion streams. So, let us neglect for a moment the source term and consider the advection equation. The ratio of the ‘‘Nernst velocity’’ \mathbf{u}_N to the ‘‘charge velocity’’ \mathbf{u} is, by an order of magnitude:

$$\frac{u_N}{u} \sim \frac{c\alpha_{\perp}}{eB} \frac{|\nabla T_e|}{v} \sim \frac{c\alpha_{\perp} T_e}{eBLv}. \quad (15)$$

For weak magnetization, according to Eq. (3), this yields:

$$\frac{u_N}{u} \sim \frac{\lambda_{ei} v_{Te}}{Lv}. \quad (16)$$

For strong magnetization, according to Eq. (4), Eq. (15) yields

$$\frac{u_N}{u} \sim \frac{\rho_e^2 v_{Te}}{\lambda_{ei} Lv}, \quad (17)$$

or, numerically,

$$\frac{u_N}{u} \sim 7 \cdot 10^{-10} \frac{Z^2 n_i (cm^{-3})}{B^2 (kG) L (cm) v (cm/s) \sqrt{T_e (eV)}}. \quad (18)$$

For the set of parameters of Table 1, the transition from low to high magnetization occurs for a magnetic field of approximately 2 to 3 kG. Such a field is too weak to cause significant modification of the ion trajectories (it corresponds to the ion gyroradius $\rho_i \sim 10$ cm), and its pressure is orders of magnitude less than the plasma pressure. We then consider the opposite case of a strong magnetization, $B > 3$ kG. In this case, one can check that the ratio u_N/u is less than 1, and one can neglect the effect of the Nernst term on

advection. We therefore arrive at the problem of the magnetic field advection by the flow of some imaginary perfectly conducting fluid,

$$\partial \mathbf{B} / \partial t = \nabla \times [\mathbf{u} \times \mathbf{B}] + \mathbf{S}, \quad (19)$$

with the velocity field \mathbf{u} determined by Eq. (9).

III. STREAMLINES OF THE EFFECTIVE FLOW

We consider two oppositely-directed plasma streams generated by small-scale sources. This imitates the conditions in experiments of the type described in Refs. [1-3]. The initial size is determined by the diameter of the driving laser focal spot, which is indeed much smaller than the length-scale L . So, in the interaction region the streams can be considered as being generated by point sources. The flows then are diverging spherically [8], with the velocities in each stream directed radially away from the corresponding source (Fig. 1).

For steady-state flows, the radial particle flux decreases as $1/R^2$ where R is the distance from each source. We will allow for variation of the flux with the polar angle ϑ ,

$$q_R(R, \vartheta) = \frac{Q(\vartheta)}{R^2}, \quad q_\vartheta = q_\varphi = 0. \quad (20)$$

The angular dependence will be approximated by the function $Q \propto \exp[-K(1 - \cos \vartheta)]$, where the parameter K characterizes the angular divergence. For example, a stream that has a half-max width of 30° corresponds to $K=5.17$; of 45° , to $K=2.37$; of 60° , to $K=1.39$; and isotropic distribution into half-space, to $K=0$. The velocity in the steady-state flow is assumed to be constant, v_0 , independent of the radius and angle. The angular variation of the particle flux is related to the angular variation of the density. Equation (20) describes one of the flows, with R measured from its origin and ϑ measured from the normal. The opposite flow will be described analogously, with the obvious change of origin and opposite direction of the normal.

To describe the shape of the streamlines, it is more convenient to use cylindrical coordinates, with the origin situated in the midplane between the sources and the axis z directed along the system axis; the origin then is situated halfway between the sources. The radial distance from the axis in cylindrical coordinates is denoted by r . In further calculations we use the distances r and z normalized to the half-length between the sources, L . In other words, the sources are situated at $z = \pm 1$. With that, the velocity field \mathbf{u} becomes:

$$u_r = \frac{Q_0 r}{n_e} \times \left[\frac{1}{(r^2 + (z+1)^2)^{3/2}} \exp - K \left[1 - \frac{z+1}{\sqrt{r^2 + (z+1)^2}} \right] + \frac{f}{(r^2 + (z-1)^2)^{3/2}} \exp - K \left[1 + \frac{z-1}{\sqrt{r^2 + (z-1)^2}} \right] \right], \quad (21)$$

$$u_z = \frac{Q_0}{n_e} \times \left[\frac{z+1}{(r^2 + (z+1)^2)^{3/2}} \exp\left[-K \left[1 - \frac{z+1}{\sqrt{r^2 + (z+1)^2}}\right]\right] + \frac{f(z-1)}{(r^2 + (z-1)^2)^{3/2}} \exp\left[-K \left[1 + \frac{z-1}{\sqrt{r^2 + (z-1)^2}}\right]\right] \right]. \quad (22)$$

The parameter f accounts for a possible asymmetry of the streams: $f < 1$ means that the upper flow is weaker than the lower one.

Streamlines of this flow are a solution of the differential equation

$$\frac{dr}{u_r} = \frac{dz}{u_z}. \quad (23)$$

Maps of the streamlines for several divergence angles are shown in Fig. 2. The lower right figure corresponds to the upper stream being two times weaker than the lower one, $f=0.5$. One sees that the effective flow stagnates on the axis and spreads sideways. As we will see in the next section, this has a significant effect on the magnetic field structure.

IV. MAGNETIC FIELD ADVECTION

As an example of the effect that the effective flow may have on the evolution of the magnetic field, we discuss the system shown in Fig. 1. As the laser pulses impinge upon the surface of the target, two clouds of hot plasma are formed near the target. It is this stage where the $\nabla n_e \times \nabla T_e$ mechanism of magnetic field generation is most efficient, due to the high temperatures and small length-scales.

The magnetic field generated by this mechanism in an axisymmetric plasma has only an azimuthal (φ) component B_φ . For non-singular distributions of temperature and density the field is zero on the axis, then grows with radius and finally disappears at a scale of the size of the focal spot.

Using standard vector analysis equations, one can present Eq. (19) as:

$$\frac{\partial B_\varphi}{\partial t} = -\frac{\partial}{\partial r}(B_\varphi u_r) - \frac{\partial}{\partial z}(B_\varphi u_z) + S_\varphi. \quad (24)$$

It can be reduced to the continuity equation for the quantity $C_\varphi = B_\varphi / r$:

$$\frac{\partial C_\varphi}{\partial t} = -\frac{1}{r} \frac{\partial}{\partial r}(C_\varphi r u_r) - \frac{\partial}{\partial z}(C_\varphi u_z) + \frac{S_\varphi}{r}. \quad (25)$$

Outside the zone near the target, the source of the magnetic field is weak, due to lower temperatures and larger length-scales, and the source term can be dropped. The evolution of the field is then determined mainly by advection.

The continuity equation (10) for the axisymmetric flow becomes

$$\frac{\partial n_e}{\partial t} = -\frac{1}{r} \frac{\partial}{\partial r}(n_e r u_r) - \frac{\partial}{\partial z}(n_e u_z) \quad (26)$$

Comparing it with Eq. (25), one concludes that outside the source region, for every Lagrange element, $C_\varphi / n_e = \text{const}$, or $B_\varphi / n_e r = \text{const}$. This is a frozen-in condition for the axisymmetric flow. It can be also derived from simple intuitive arguments as follows. Consider the evolution of a magnetic fluxtube of a small cross-section ΔS . It forms a

torus surrounding the axis of the system. The magnetic flux $\Delta\Phi$ through the tube does not change and, therefore, the field strength varies in inverse proportion to the cross-section, $B_\varphi = \Delta\Phi / \Delta S$. On the other hand, the number of electrons inside the tube, $\Delta N_e = 2\pi r n_e \Delta S$, also does not change. Therefore, the parameter $B_\varphi / n_e r$ remains constant through the motion of the tube:

$$B_\varphi / n_e r = \text{const} . \quad (27)$$

In the situation of identical streams ($f=1$), the mid-plane serves as an impermeable boundary for the effective charge flow and, by virtue of the frozen-in condition, the field generated near the lower target cannot penetrate beyond this plane. The same is true for the field generated by the upper target.

If only one stream is present, then the streamlines are straight lines emerging from an area of the size of a focal spot radius. The ensuing stream then reaches the midplane at a radius determined by straight streamlines (Fig.3). Conversely, in the presence of two flows, the streamlines deviate toward much larger radii (Fig. 3). The density also increases compared to a single stream, roughly by a factor of two, due to the overlap with the second stream. The product of the radius and density is significantly greater than for the single stream. Equation (27) then tells us that the presence of a zone near the midplane where the flow becomes almost radial, together with the density increase related to the contribution of the second stream, leads to a large increase of the magnetic field near the midplane compared to a single flow. The field strength near the midplane will be still much less than the field in the generation zone but much higher than it would have been if only one flow was present.

The same happens, of course, on the other side of the midplane, leading to the formation of two flattened zones of a strong magnetic field near the midplane. Note that, by symmetry arguments, the field generated by the $\nabla n_e \times \nabla T_e$ mechanism in the upper half-space will have an opposite sign with respect to the field in the lower half-space, thereby creating a natural experimental platform for studies of magnetic reconnection, albeit in a somewhat exotic setting (see below).

The specific value of the magnetic field enhancement factor depends on the details of the flow spatial and temporal characteristics. To find this number, one has to follow a given Lagrange fluid element along the streamline, thereby following r and z . The density at the instantaneous location of the fluid element is determined simply by Eq. (6). Then, using Eq. (25), one finds the field in a desired location and compares it to the field produced at the same point by a single flow.

To give an example of such analysis, we consider streams with a half angular width of 45° and assume the following radial distribution of the magnetic field over the radius halfway between the lower target and midplane (i.e., along the dotted lower line in Fig. 3):

$$B = 8B_0 r \exp(1 - 8r) \quad (28)$$

The distances here and in the equations below are normalized to the length-scale L , Fig. 1. This distribution is illustrated by a green line (#1) in Fig. 4. Then, for a single flow, using Eq. (27), one finds that the radial distribution near the midplane, at a distance of $\Delta z = 0.1L$, is determined by the blue curve (#2) in Fig. 4. The maximum field is now approximately two times lower than B_0 . If, however, we have two counter-propagating identical flows, with streamlines shown in Fig. 2b, the magnetic field near the midplane,

for $\Delta z = 0.1L$, becomes stronger, and its radial distribution widens (curve #3 Fig. 4). Closer to the midplane, $\Delta z = 0.05L$, a further widening occurs (magenta curve in Fig. 4). In other words, a flattened structure of the enhanced magnetic field is formed on each side of the midplane, with the fields on opposite sides having opposite signs.

The absolute value of the field depends on the sources that have produced the field near the targets. For the experiments of the type [1-3], the laser intensities and focal spot sizes are comparable to those in Ref. [17], where a detailed characterization of the field was produced. So, we assume that the field in the generation area is ~ 50 T and the radius of this area is ~ 300 μm . Then, at the distance of $L/2 \sim 2.5$ mm the field strength in our model would be ~ 8 times less, i.e., ~ 6 T. For a single flow it would further drop to ~ 3 T at a distance $L \sim 5$ mm. However, in the presence of two flows, it will be enhanced by the stagnation flow and increase by a factor ~ 2 , to the value ~ 12 T. Importantly, this enhancement zone will be flattened near the midplane, due to the shape of the effective flow, with a radius significantly greater than its thickness.

V. DISCUSSION

We have derived the frozen-in conditions for two interpenetrating weakly-collisional plasma streams and have shown that for a broad range of parameters the field is frozen into the ion charge flow. The latter forms a set of streamlines that possesses a singular surface “impermeable” to this effective flow, although the ions of each stream pass through it freely. In the vicinity of this surface the effective flow is diverted sideways, to larger radii. The magnetic field therefore is compressed near this surface and becomes significantly higher than it would have been in a single flow. The field distribution experiences also a “flattening” near this plane.

Our model describes the evolution of the magnetic field subsequent to its advection by the plasma flow out of the generation zone near the target, but it does not predict the magnitude of the field. If the field is generated by the $\nabla n_e \times \nabla T_e$ mechanism, then it can be found by the solving 2-dimensional magnetohydrodynamic equations near the targets. Helpfully, the presence of the second stream near the target can be ignored, as its density there is very low.

If the magnetic field is generated by the $\nabla n_e \times \nabla T_e$ mechanism, it has an opposite polarity on the two sides of the separating surface. This creates a natural platform for the study of magnetic reconnection (see Ref. [18] for a general review of magnetic reconnection). For realistic values of the magnetic field that one can expect in the vicinity of the separating surface, the size of the ion gyro-orbit is large compared to the thickness of this zone, so that the ion streams react only weakly to the magnetic fields. As a result, the ions enter the problem only via the quasineutrality condition, providing a known neutralizing background. The reconnection itself would occur in the electron fluid. Such a setting allows one to test various reconnection models in a situation in which the reconnection occurs in the electron fluid, with the ions providing a fixed neutralizing background.

Acknowledgment

Work performed for U.S. DoE by LLNL under Contract DE-AC52-07NA27344.

APPENDIX. Tilted targets

In this appendix we illustrate the shape of the stagnation surfaces for the case where the targets are tilted with respect to each other, as shown in Fig. 5a. The distances are normalized to the half-distance between the flow origins, i.e. to L , Fig. 5a. The tilt angles are γ_L and γ_U for the lower and the upper target, respectively.

In three-dimensions, these stagnation surfaces are non-planar and thereby hard to illustrate. We therefore consider in this section two-dimensional flows in the x - y plane. We keep the assumption that the velocity is constant, and that the angular dependence of the flux is caused by the angular dependence of the density.

In Fig. 5b, the shape of the streamlines is shown for the half-divergence angle of 60° , $\gamma_L=\gamma_U=45^\circ$, for the streams of identical intensity. The separating surface goes from the lower left to the upper right corner. Intersecting it is a singular streamline whose intersection with the separating surface determines the point where $\mathbf{u}=0$. The latter line in the model under consideration turns out to always be a straight line connecting the origins of the flows. In Fig. 5c, we illustrate the situation with $\gamma_L=\gamma_U=45^\circ$, but half-divergence angle of 30° and the lower stream two times weaker than the upper stream. The separating surface is now non-planar and shifted closer to the weaker source.

Fig.5 shows that the flattened structures of the magnetic field formed near the “impermeable” surface can have a variety of orientations, depending on the geometry of the targets and the mutual intensity of the flows.

References

- [1] H.-S. Park, D.D. Ryutov, J.S. Ross, N.L. Kugland, S.H. Glenzer, C. Plechaty, S.M. Pollaine, B.A. Remington, A. Spitkovsky, L. Gargate, G. Gregori, A. Bell, C. Murphy, Y. Sakawa, Y. Kuramitsu, T. Morita, H. Takabe, D.H. Froula, G. Fiksel, Miniati, M. Koenig, A. Ravasio, A. Pelka, E. Liang, N. Woolsey, C.C. Kuranz, R.P. Drake, and M.J. Grosskopf. “Studying astrophysical collisionless shocks with counterstreaming plasmas from high power lasers,” *High Energy Density Physics* **8**, 38 (2012).
- [2] N. L. Kugland, D. D. Ryutov, P.-Y. Chang, R. P. Drake, G. Fiksel, D. H. Froula, G. Gregori, M. Grosskopf, M. Koenig, Y. Kuramitsu, C. Kuranz, M. C. Levy, E. Liang, J. Meinecke, F. Miniati, T. Morita, A. Pelka, C. Plechaty, R. Presura, A. Ravasio, B. A. Remington, B. Reville, J. S. Ross, Y. Sakawa, A. Spitkovsky, H. Takabe, H.-S. Park. “Self-organized electromagnetic field structures in laser-produced counterstreaming plasmas.” *Nature Physics*, **8**, 809 (2012).
- [3] J.S. Ross, S.H. Glenzer, P. Amendt, R. Berger, L. Divol, N.L. Kugland, O.L. Landen, C. Plechaty, B. Remington, D. Ryutov, W. Rozmus, D.H. Froula, G. Fiksel, C. Sorce, Y. Kuramitsu, T. Morita, Y. Sakawa, H. Takabe, R.P. Drake, M. Grosskopf, C. Kuranz, G. Gregori, J. Meinecke, C.D. Murphy, M. Koenig, A. Pelka, A. Ravasio, T. Vinci, E. Liang, R. Presura, A. Spitkovsky, F. Miniati, and H.-S. Park. “Characterizing counter-streaming interpenetrating plasmas relevant to astrophysical collisionless shocks” *Phys. Plasmas*, **19**, 056501 (2012).
- [4] R.Z. Sagdeev. “Nonlinear plasma theory.” In: *Reviews of plasma physics* v. 4, M.A. Leontovich, Ed., Consultants Bureau, N-Y (1969).
- [5] T.N. Kato and H. Takabe. “Nonrelativistic Collisionless Shocks in Unmagnetized Electron-Ion Plasmas.” *Astrophys. J.* **681**, L93–L96 (2008).
- [6] T.N. Kato and H. Takabe. “Electrostatic and electromagnetic instabilities associated with electrostatic shocks: Two-dimensional particle-in-cell simulation.” *Phys. Plas.*, **17**, 032114 (2010).
- [7] L. Gargate, A. Spitkovsky. “Ion acceleration in non-relativistic astrophysical shocks.” *Astrophys. J.* **744**, 67 (2012).
- [8] R.P. Drake and G. Gregori. “Design considerations for unmagnetized collisionless-shock measurements in homologous flows.” *Astrophys. J.*, **749**, 171 (2012).
- [9] D.D. Ryutov, N.L. Kugland, H.-S. Park, S.M. Pollaine, B.A. Remington, J.S. Ross. “Collisional current drive in two interpenetrating plasma jets.” *Phys. Plasmas*, **18**, 104504 (2011).
- [10] D.D. Ryutov, N.L. Kugland, H.-S. Park, C. Plechaty, B.A. Remington, J.S. Ross. “Intra-Jet Shocks in Two Counter-Streaming, Weakly Collisional Plasma Jets.” *Phys. Plasmas*, **19**, 074501 (2012).
- [11] K. Shigemori, R. Kodama, D.R. Farley, T. Koase, K.G. Estabrook, B.A. Remington D.D. Ryutov, Y. Och, H. Azechi, J. Stone, N. Turner. “Experiments on radiative collapse in laser-produced plasmas relevant to astrophysical jets.” *Phys Rev E*, **62**, 8838 (2000).
- [12] J.M. Foster, B.H. Wilde, P.A. Rosen et al. “High-energy-density laboratory astrophysics studies of jets and bow shocks.” *ApJ*, **634**, L77 (2005)
- [13] J. A. Stamper. “Review on spontaneous magnetic-fields in laser-produced plasmas - phenomena and measurements.” *Laser and Particle Beams* **9**, 841 (1991).

- [14] S.I. Braginski. In: *Reviews of Plasma Physics*, edited by M. A. Leontovich (Consultants Bureau, New York), Vol. 1, p. 205 (1965).
- [15] L. Willingale, A.G.R. Thomas, P.M. Nilson, M.C. Kaluza, S. Bandyopadhyay, A.E. Dangor, R.G. Evans, P. Fernandes, M.G. Haines, C. Kamperidis, R.J. Kingham, S. Minardi, M. Notley, C.P. Ridgers, W. Rozmus, M. Sherlock, M. Tatarakis, M.S. Wei, Z. Najmudin, K. Krushelnik. "Proton probe measurement of fast advection of magnetic fields by hot electrons." *Plasma Phys. Contr. Fusion*, **53**, 124026 (2011).
- [16] A.V. Gordeev, A. S. Kingsep, and L. I. Rudakov, "Electron magnetohydrodynamics." *Phys. Rep.* **243**, 215 (1994).
- [17] C. K. Li, F. H. Séguin, J. A. Frenje, J. R. Rygg, R. D. Petrasso, R. P. J. Town, P. A. Amendt, S. P. Hatchett, O. L. Landen, A. J. Mackinnon, P. K. Patel, V. A. Smalyuk, T. C. Sangster, and J. P. Knauer, "Measuring E and B fields in laser-produced plasmas with monoenergetic proton radiography" *Phys. Rev. Lett.* **97**, 135003 (2006).
- [18] M. Yamada, R. Kulsrud, H. Ji. "Magnetic reconnection." *Rev. Mod. Phys.*, **82**, 603 (2010).

Table 1 Parameters of each of the streams in the midpoint between the targets for fully stripped carbon

Parameter	Ion density, n_i, cm^{-3}	Ion flow velocity, $v, \text{cm/s}$	Ion kinetic energy, W_i, keV	Ion temp., T_i, keV	Electron temp., T_e, keV	Spatial scale, L, cm	Temporal scale, $\tau=L/v, \text{ns}$
Value	10^{18}	10^8	60	1	1	0.5	5

Table 2 Derived parameters

Parameter	Notation	Value
Inter-stream ion collision length ^{a)}	λ_{ii}^*	10 cm
Intra-stream ion collision length	λ_{ii}	30 μm
Electron-ion collision length	λ_{ei}	0.05 cm
Ion thermal velocity	v_{Ti}	$1.4 \times 10^7 \text{ cm/s}$
Electron thermal velocity	v_{Te}	$2 \times 10^9 \text{ cm/s}$
Magnetic diffusivity	D_M	$10^3 \text{ cm}^2/\text{s}$
Magnetic Reynolds number	$Re_M = Lv/D_M$	5×10^4
Thermal beta for electron gas	$\beta_T \equiv 2Zn_iT_e / p_M$ (p_M =magnetic pressure)	20, for a magnetic field of 10 T

^{a)} We use an asterisk to mark the collisions between two streams, vs. in-stream collisions.

Figure captions

Fig. 1 The geometry of the problem. Arrows show streamlines of the diverging ion flow in the vicinity of the targets. The size of the sources is assumed to be small compared to L , consistent with recent experiments.

Fig. 2 Streamlines of the effective flow: a) half angular width of 30 degrees; b) half angular width of 60 degrees; c) half angular width of 90 degrees (isotropic flow); d) half angular width of 60 degrees and $f=0.5$ (the upper jet is 2 times weaker than the lower one).

Fig. 3 Comparison of magnetic field advection for a single and a double flow. The lower dotted line corresponds to a cross-section half-way between the midplane and the lower target. Streamlines of the single flow (dashed straight line) and effective flow (solid line) are virtually indistinguishable below this cross-section. The radial field distributions here are also essentially the same for single flow and the counterstreaming flows. This distribution is shown in Fig. 4, curve 1. In the case of a single flow, the magnetic field decreases significantly from this cross-section to that near the midplane (the dotted line at a distance of $0.1L$ from the midplane), see curve 2 in Fig. 4. Conversely, for the counterstreaming flows the field at the distance of $0.1L$ becomes higher than the field at the distance of $0.5L$ from the target.

Fig. 4 The magnetic field radial distribution: 1 – half-way between the lower target and the midplane; 2 – $\Delta z = 0.1L$ below the midplane for a single flow; $\Delta z = 0.1L$ below the midplane for symmetric counterstreaming flows; $\Delta z = 0.05L$ below the midplane for the symmetric counterstreaming flows. All the fields are normalized to the maximum value B_0 of the magnetic field for the curve #1.

Fig.5 Streamlines for tilted targets: a) Target orientation; b) Streamlines for $\gamma_L=\gamma_U=45^\circ$, and half-divergence angle of 60° . The axes of the flows are shown by arrows. Flows have the same density. c) Streamlines for $\gamma_L=\gamma_U=45^\circ$, and half-divergence angle of 30° . The lower stream is two times less dense than the upper one.

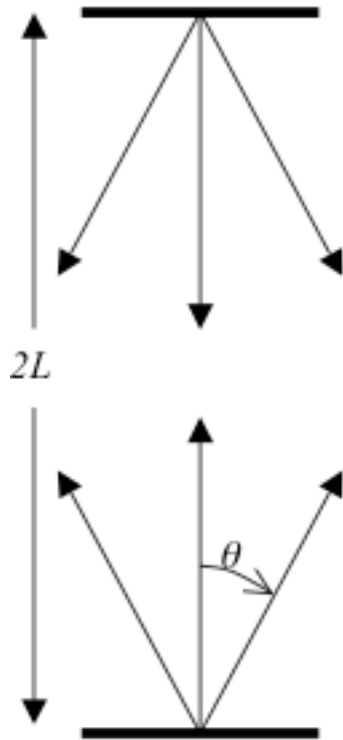


Fig.1

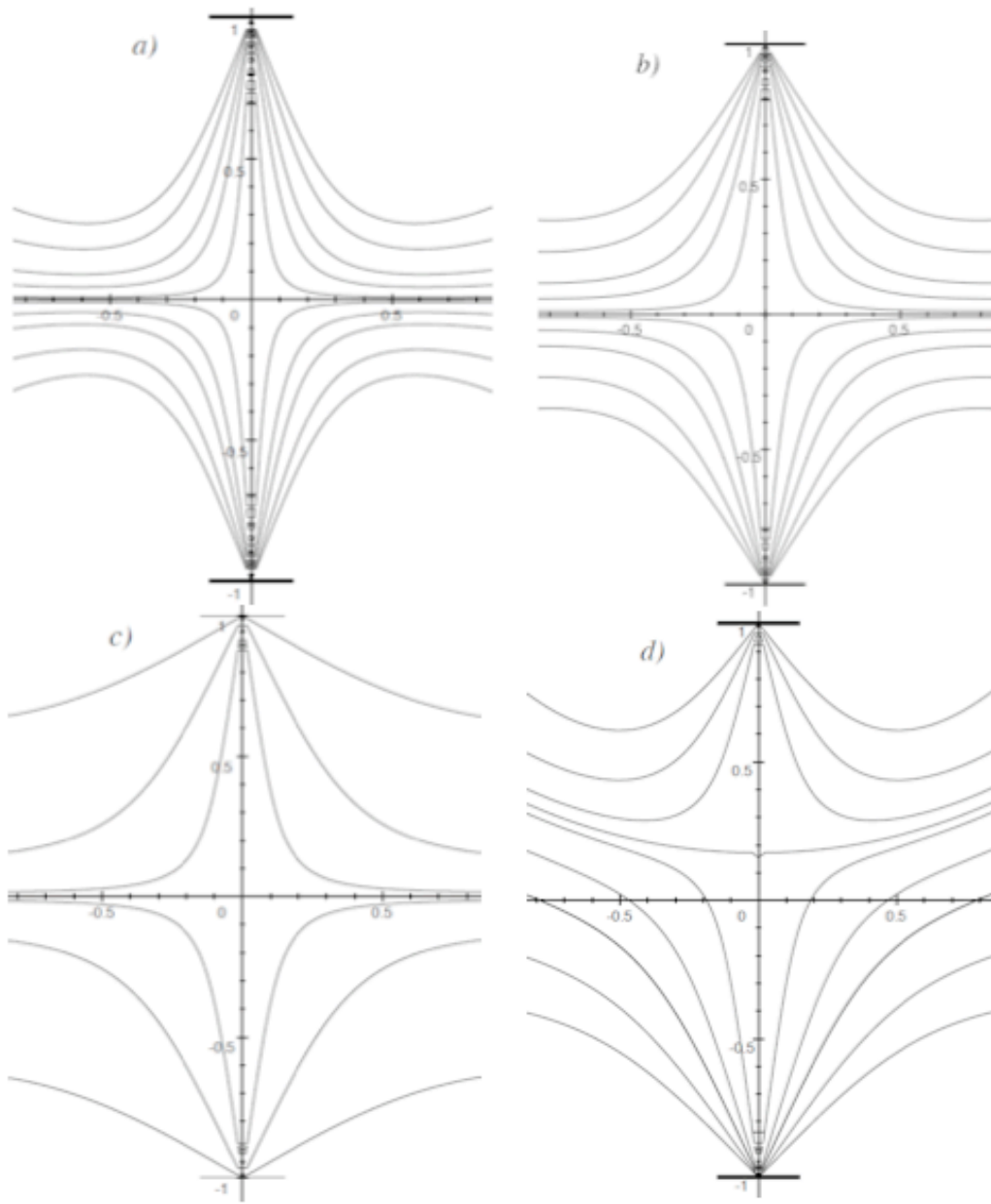


Fig. 2

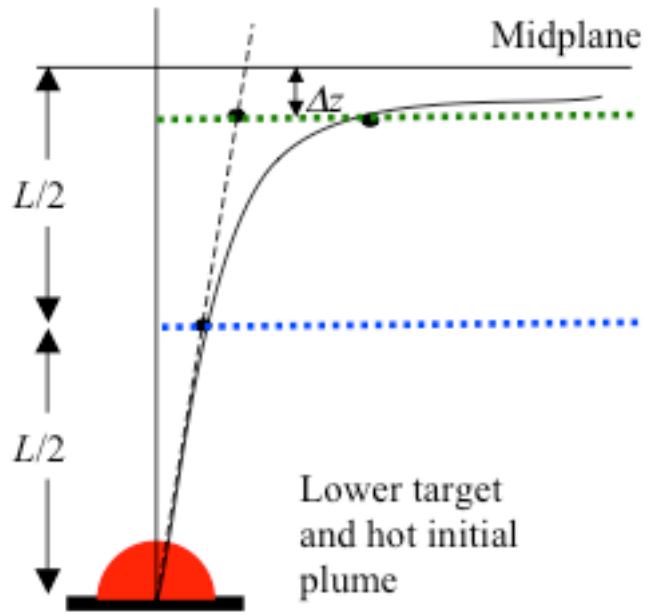


Fig.3

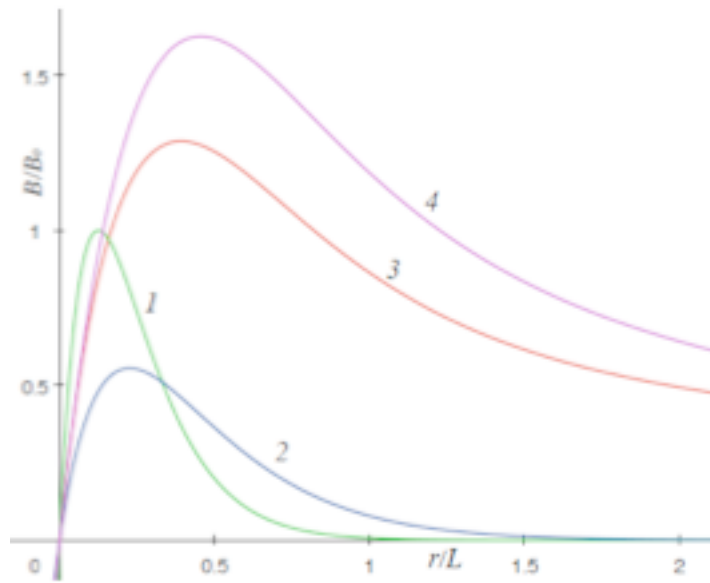


Fig.4

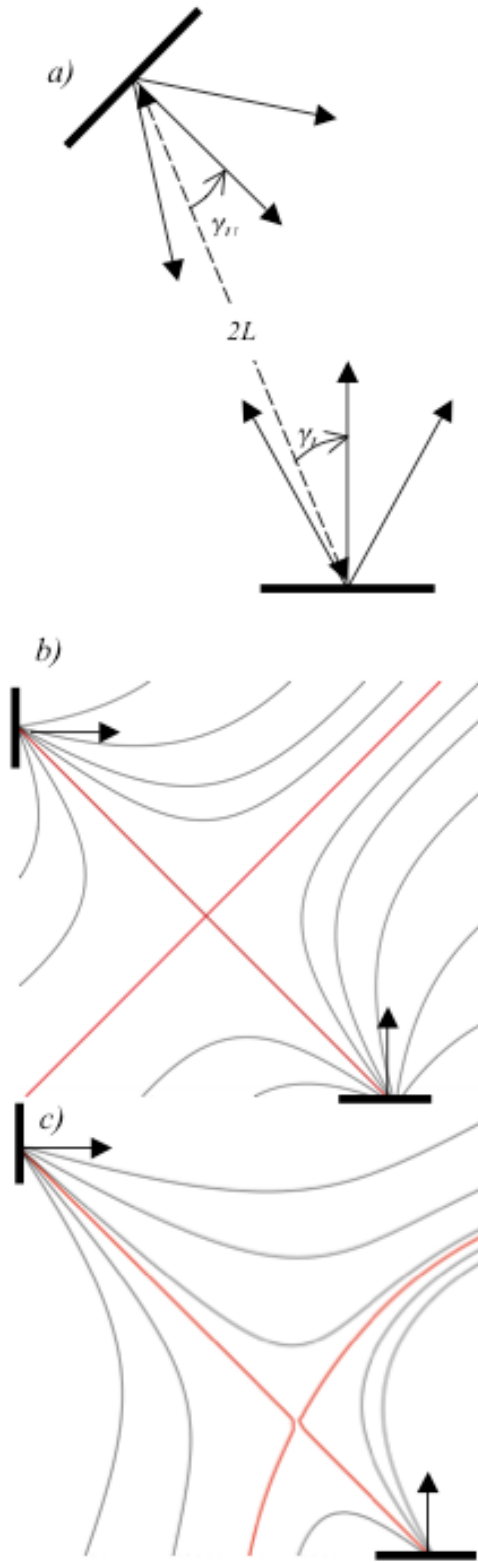


Fig. 5